

Excellent thermal stability of Al₂O₃ / ZrO₂ / Al₂O₃ stack structure for metal–oxide–semiconductor gate dielectrics application

Hyo Sik Chang, Sanghun Jeon, Hyunsang Hwang, and Dae Won Moon

Citation: [Applied Physics Letters](#) **80**, 3385 (2002); doi: 10.1063/1.1477266

View online: <http://dx.doi.org/10.1063/1.1477266>

View Table of Contents: <http://scitation.aip.org/content/aip/journal/apl/80/18?ver=pdfcov>

Published by the [AIP Publishing](#)

Articles you may be interested in

[Atomic layer deposited HfO₂ / HfSi_xO_yN_z stacked gate dielectrics for metal-oxide-semiconductor structures](#)
J. Vac. Sci. Technol. B **25**, 1922 (2007); 10.1116/1.2811707

[Effects of plasma nitridation of Al₂O₃ interlayer on thermal stability, fixed charge density, and interfacial trap states of HfO₂ gate dielectric films grown by atomic layer deposition](#)
J. Appl. Phys. **94**, 1898 (2003); 10.1063/1.1590418

[Ultrathin nitrided-nanolaminate \(Al₂O₃ / ZrO₂ / Al₂O₃ \) for metal–oxide–semiconductor gate dielectric applications](#)
J. Vac. Sci. Technol. B **20**, 1143 (2002); 10.1116/1.1481864

[Miscibility of amorphous ZrO₂ – Al₂O₃ binary alloy](#)
Appl. Phys. Lett. **80**, 2374 (2002); 10.1063/1.1459765

[Electrical characteristics and thermal stability of n + polycrystalline- Si/ZrO₂ /SiO₂ /Si metal–oxide–semiconductor capacitors](#)
J. Appl. Phys. **91**, 414 (2002); 10.1063/1.1425073

An advertisement for Keysight B2980A Series Picoammeters/Electrometers. The ad features a photograph of the device, which is a handheld electronic instrument with a screen and various buttons. To the left of the device, the text reads: 'Confidently measure down to 0.01 fA and up to 10 PΩ' and 'Keysight B2980A Series Picoammeters/Electrometers'. Below this text is a red button with the text 'View video demo'. To the right of the device is the Keysight Technologies logo, which consists of a stylized red waveform and the text 'KEYSIGHT TECHNOLOGIES'.

Excellent thermal stability of $\text{Al}_2\text{O}_3/\text{ZrO}_2/\text{Al}_2\text{O}_3$ stack structure for metal–oxide–semiconductor gate dielectrics application

Hyo Sik Chang, Sanghun Jeon, and Hyunsang Hwang^{a)}

Department of Materials Science and Engineering, Kwangju Institute of Science and Technology, Kwangju 500-712, Korea

Dae Won Moon

Nano Surface Group, Korea Research Institute of Standards and Science, Daejeon 305-600, Korea

(Received 29 November 2001; accepted for publication 9 March 2002)

The thermal stability of a nanolaminate ($\text{Al}_2\text{O}_3/\text{ZrO}_2/\text{Al}_2\text{O}_3$) gate stack prepared by atomic layer chemical vapor deposition was investigated using medium-energy ion scattering spectroscopy, and x-ray photoelectron spectroscopy. We observed that the structure was stable up to 1000 °C under ultrahigh vacuum conditions. However, annealing in a nitrogen or oxygen ambient at 1 atm yielded the formation of an interfacial Zr–Al silicate layer at much lower temperatures. The growth of the interfacial silicate layer could be significantly reduced during furnace annealing via the use of plasma nitridation. © 2002 American Institute of Physics. [DOI: 10.1063/1.1477266]

As the gate oxide thickness of a metal–oxide–semiconductor field-effect transistor device was scaled down to below 1.5 nm, conventional thermal SiO_2 is no longer applicable because of the excess direct tunneling leakage current. Conventional high- k candidates, such as SrTiO_3 , Ta_2O_5 , TiO_2 , Y_2O_3 , ZrO_2 , HfO_2 , Zr silicate, and Hf silicate, have been investigated as alternative gate dielectric materials.¹ However, considering the thermal stability and dielectric constant, ZrO_2 , HfO_2 and their silicates are the most promising.^{1–3}

Based on phase diagrams and thermodynamic predictions, an excellent thermal stability of ZrO_2 on silicon can be predicted. However, the formation of an interfacial oxide layer and silicide at the ZrO_2/Si interface has been reported.^{2–4} In addition, ZrO_2 films which are directly deposited on a HF-last $\text{Si}(001)$ surface caused an island-type nucleation which degrades film roughness and leakage current.^{4,5} Although a single- ZrO_2 layer structure is preferred for the process simplicity, the degradation of thermal stability was observed for ultrahigh vacuum (UHV) annealing at 1000 °C.⁴ Therefore, the introduction of an Al_2O_3 layer has several advantages such as the formation of an atomically flat film and robustness against the silicide formation at 1000 °C.^{5–7}

In this letter, we report the investigation of the effect of high-temperature annealing ambients such that UHV and 1 atm nitrogen on the thermal stability of a nanolaminate ($\text{Al}_2\text{O}_3/\text{ZrO}_2/\text{Al}_2\text{O}_3$) structure. In addition, to improve the thermal stability, we evaluated the effect of plasma nitridation which provides the sufficient stability at a high-temperature annealing.

A uniform ultrathin $\text{Al}_2\text{O}_3/\text{ZrO}_2/\text{Al}_2\text{O}_3$ layered structure was deposited on a 4 in. $\text{Si}(001)$ wafer by atomic layer chemical vapor deposition. After standard cleaning, an ultrathin (less than 1 nm thick) amorphous Al_2O_3 buffer layer was deposited using trimethylaluminum and H_2O vapor as

source gases. Then, a 4 nm-thick ZrO_2 layer was prepared using ZrCl_4 and H_2O vapor as source gases. Finally, a 0.5 nm-thick Al_2O_3 buffer layer was deposited on top of the ZrO_2 . The substrate temperature and the process pressure were 300 °C and 1 Torr, respectively. After the deposition of a 150 nm-thick layer of Pt, metal–oxide–semiconductor (MOS) devices with a gate area of $9 \times 10^{-6} \text{ cm}^2$ were defined by photolithography and etching. The electrical properties of the nanolaminate film were characterized by capacitance–voltage ($C-V$), and current density–voltage ($J-V$) measurements. For the thermal stability measurements, samples were transferred to the UHV-medium-energy ion scattering (MEIS) system with sample heating capabilities.

MEIS analysis was accomplished with a 100 keV proton beam in the double alignment in order to reduce contributions from the crystalline Si substrates, allowing the deconvolution of spectra into contributions from the bottom Al_2O_3 , the underlying SiO_2 , and the interfacial Si signals.⁸ The incident ions were along $[111]$ in the (011) plane and the scattered ions were along $[00\bar{1}]$ with a scattering angle of 125°. The energy resolution of electrostatic energy analyzer of MEIS is almost single atomic layer depth resolution in the near surface.⁹ During MEIS experiments, the specimen was moved and the H^+ dose was maintained below $2 \times 10^{15} \text{ cm}^{-2}$ in order to prevent damage. In addition to MEIS, other powerful analytical techniques, such as x-ray photoelectron spectroscopy (XPS), high-resolution transmission electron microscopy (HRTEM), and electrical measurements, were used in this study.

Figure 1 shows a proton backscattering energy spectrum from the as-deposited and vacuum-annealed nanolaminate film. Using a simulation program for scattering analysis, the best-fit result for the compositional depth profile was obtained as shown in the inset of Fig. 1.^{10,11} For the bottom Al_2O_3 film deposited on the Si substrate, a 1.4 ± 0.3 nm thick interfacial silicate layer was found, which is composed of Zr, Al, Si, and O. Based on the contrast difference in HRTEM, a 0.6 nm-thick interfacial layer was identified as being related

^{a)}Electronic mail: hwanghs@kjist.ac.kr

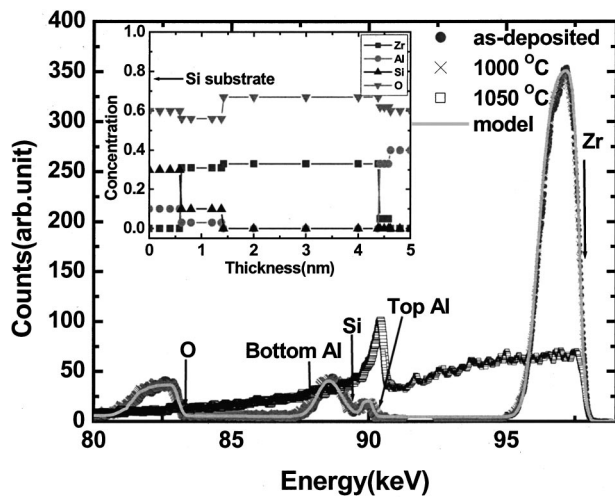


FIG. 1. MEIS energy spectra for $\text{Al}_2\text{O}_3/\text{ZrO}_2/\text{Al}_2\text{O}_3$, layered films on Si(001) after high-temperature UHV annealing. Negligible degradation of the MEIS spectra was observed at annealing temperatures up to 1000 °C. The Zr, Si, Al, and O concentration profiles used in the model are given in the inset.

to the Zr-deficient layer at the interface. In contrast, Al_2O_3 layer on top of 4 nm-thick ZrO_2 was identified as a stoichiometric Al_2O_3 film. The root-mean-square roughness was determined to be 0.14 nm.

To confirm the thermal stability, UHV annealing was performed at a pressure lower than 4×10^{-8} Torr. After UHV annealing at 1000 °C for 20 s, almost no change was observed in the MEIS spectra for the nanolaminate layer. However, UHV annealing at 1100 °C for 10 s completely decomposed the nanolaminate layer as shown in the MEIS spectra. A significant intermixing of Zr with the underlying silicon substrate was observed. In addition, a reduction in the oxygen peak intensity was found, which can be attributed to the decomposition of the oxide film. It is known that UHV annealing of a $\text{ZrO}_2/\text{SiO}_2$ stack at 1000 °C completely decomposes the oxide layer.⁴ Considering the excellent thermal stability of the Al_2O_3 buffer layer, it is possible to maintain the nanolaminate layer structure at annealing temperatures as high as 1000 °C.

To understand the effect of annealing ambient and pressure, an atmospheric pressure annealing was performed in pure O_2 and N_2 ambients. After annealing, we observed a broadening of the oxygen peak indicating the interfacial oxide growth as shown in Fig. 2. After high-temperature annealing, MEIS measurements indicated that the interfacial layer consists of Zr, Al, Si, and O. The growth of the interfacial layer became saturated roughly at 1.5 ± 0.3 nm and was insensitive to annealing ambient and conditions. The angle-resolved XPS results also show that the substantial Si—O growth can take place after annealing, as predicted in the MEIS data. The growth of the interfacial oxide layer was confirmed by the increased chemical shift component of Si 2*p* spectra in the inset of Fig. 2. A new peak appeared at high binding energy and an additional peak moved together toward higher binding energy after annealing. This shift indicates that Si—O—Si bond formation dominates the reaction during a high-temperature annealing.^{12,13} Considering the relative high silicon intensity of the annealed sample at a different take-off angle, the high surface concentration of

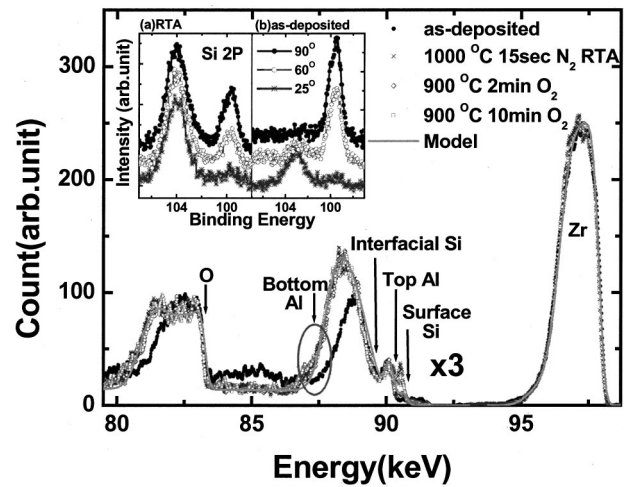


FIG. 2. Ion scattering spectra for nanolaminate films after annealing in N_2 and O_2 ambients. Due to oxidation, the growth of a about 1.5 nm-thick interfacial layer was confirmed by MEIS and XPS analysis.

silicon would be expected and this can be explained by the diffusion of silicon interstitial from the Si/oxide interface.^{14,15}

Since the ultrathin Al_2O_3 is not a good diffusion barrier to oxygen, a remote plasma nitridation in N_2 was carried out in order to reduce the growth of the interfacial oxide layer during annealing. According to the atomic force microscopy analysis, the surface roughness after nitridation is negligible. Figure 3 shows an ion scattering spectrum of an as-deposited and nitridated nanolaminate. After nitridation, the growth of the interfacial silicate layer was reduced during annealing in nitrogen at 700 °C for 10 min. MEIS analysis indicates that the thickness of the interfacial oxide layer of the nitridated nanolaminate was approximately 3–5 Å thinner than that of a control sample. The growth of the interfacial oxide layer indicated by the Si—O or silicate peak at 102 eV in Si 2*p* spectra was significantly lower for the nitridated sample. This is in good agreement with MEIS results.

To investigate the electrical characteristics of the dielectric, MOS capacitors with a Pt or a polycrystalline silicon electrode were fabricated. Figure 4 shows their high fre-

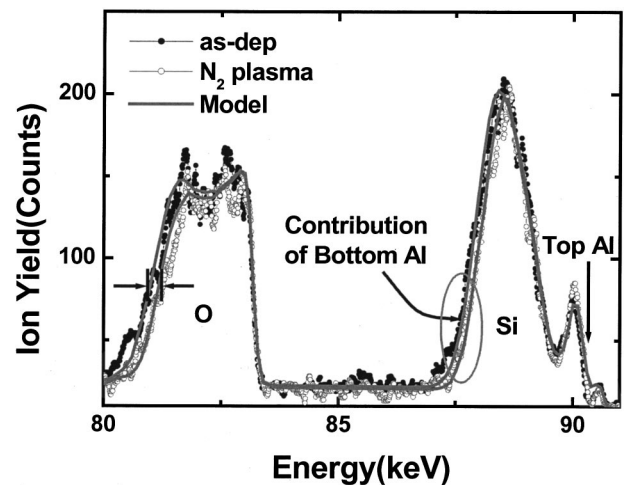


FIG. 3. MEIS energy spectra of an as-deposited and nitridated nanolaminate. After nitridation, the growth of the interfacial layer was reduced during annealing at 700 °C for 10 min.

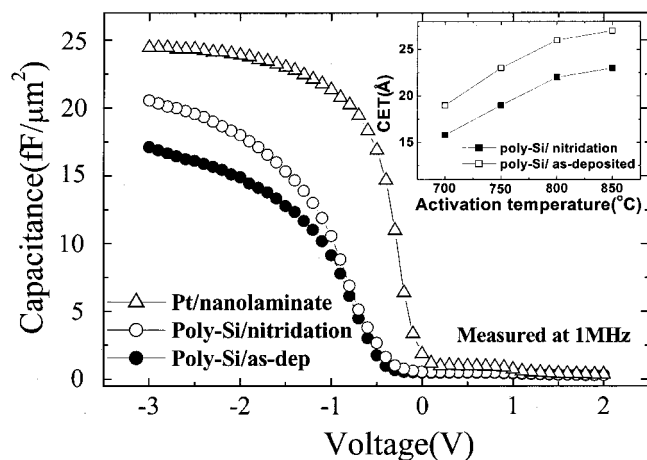


FIG. 4. $C-V$ results for as-deposited and nitrided nanolaminate. Nitrided sample shows less degradation in the accumulation capacitance. Inset shows capacitance equivalent thickness as a function of annealing temperature.

quency ($C-V$) characteristics. The degradation of the accumulation capacitance can be explained by the growth of the interfacial oxide layer. As expected, plasma nitridation of the nanolaminate sample shows less degradation of accumulation capacitance. The nitrided sample shows a higher capacitance and lower leakage current density which can be explained by less defect density.¹⁶

In summary, we investigated the microstructure properties of a nanolaminate ($\text{Al}_2\text{O}_3/\text{ZrO}_2/\text{Al}_2\text{O}_3$) layered structure and the effect of plasma nitridation on the thermal stability. We observed that the excellent thermal stability at annealing temperatures as high as 1000 °C in an UHV ambient. In contrast, a significant growth of the interfacial layer was observed in nitrogen or oxygen ambients at an annealing temperature of 900 °C. A significant improvement in the thermal stability of the nanolaminate was observed, as the result

of plasma nitridation which can be explained by a reduction in the growth of the interfacial oxide layer. Considering the excellent thermal stability and the electrical characteristics, the nanolaminate structure shows the promising results for use in high- k gate dielectric applications in the future.

The authors thank Mr. C. Werkhoven of ASM America and Dr. D. G. Park of Hynix Semiconductor Inc. for the nanolaminate sample preparations. This work was supported by the Brain Korea 21 project and the National Program for Tera Level Nano Devices through MOST.

- ¹G. D. Wilk, R. M. Wallace, and J. M. Anthony, *J. Appl. Phys.* **87**, 484 (2000).
- ²K. J. Hubbard and D. G. Schlom, *J. Mater. Res.* **11**, 275 (1996).
- ³B. W. Bush, W. H. Schulte, E. Garfunkel, T. Gustafsson, W. J. Qi, R. Nieh, and J. C. Lee, *Phys. Rev. B* **62**, R13 290 (2000).
- ⁴M. Copel, A. Gribelyuk, and E. Gusev, *Appl. Phys. Lett.* **76**, 436 (2000).
- ⁵V. V. Afanas'ev, M. Haussa, A. Stesmans, and M. M. Heyns, *Appl. Phys. Lett.* **78**, 3073 (2001).
- ⁶E. P. Gusev, M. Copel, E. Cartier, I. J. R. Baumvol, C. Krug, and M. A. Gribelyuk, *Appl. Phys. Lett.* **76**, 176 (2000).
- ⁷M. Copel, E. Cartier, E. P. Gusev, S. Guha, N. Bojarczuk, and M. Poppeler, *Appl. Phys. Lett.* **78**, 2670 (2001).
- ⁸J. F. van der Veen, *Surf. Sci. Rep.* **5**, 199 (1985).
- ⁹Y. P. Kim, S. K. Choi, H. K. Kim, and D. W. Moon, *Appl. Phys. Lett.* **71**, 3504 (1997).
- ¹⁰E. P. Gusev, H. C. Lu, T. Gustafsson, and E. Garfunkel, *Phys. Rev. B* **52**, 1759 (1995).
- ¹¹Y. Kido and T. Koshikawa, *J. Appl. Phys.* **67**, 187 (1990).
- ¹²S. Iwata and A. Ishizaka, *J. Appl. Phys.* **79**, 6653 (1996).
- ¹³H. Watanabe, *Appl. Phys. Lett.* **78**, 3803 (2001).
- ¹⁴C. Krug, E. B. O. da Rossa, R. M. C. de Almeida, J. Morais, I. J. R. Baumvol, T. D. M. Salgado, and F. C. Stedile, *Phys. Rev. Lett.* **85**, 4120 (2000).
- ¹⁵M. Kundu, N. Miyata, and M. Ichikawa, *Appl. Phys. Lett.* **78**, 1517 (2001).
- ¹⁶S. Jeon, C.-J. Choi, T.-Y. Seong, and H. Hwang, *Appl. Phys. Lett.* **79**, 245 (2001).